Three-dimensional models of 14α-sterol demethylase (Cyp51A) from and : an insight into differences in voriconazole interaction

Laura Alcazar-Fuoli, Isabel Cuesta, Juan L. Rodriguez-Tudela, Manuel Cuenca-Estrella, Dominique Sanglard, Emilia Mellado

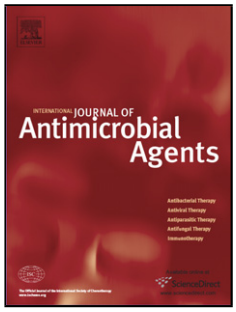

Title: Three-dimensional models of 14α-sterol demethylase (Cyp51A) from *Aspergillus lentulus* and *Aspergillus fumigatus*: an insight into differences in voriconazole interaction

Authors: Laura Alcazar-Fuoli, Isabel Cuesta, Juan L. Rodriguez-Tudela, Manuel Cuenca-Estrella, Dominique Sanglard, Emilia Mellado

PII: S0924-8579(11)00260-3
DOI: doi:10.1016/j.ijantimicag.2011.06.005
Reference: ANTAGE 3644

To appear in: *International Journal of Antimicrobial Agents*

Received date: 23-11-2010
Revised date: 31-5-2011
Accepted date: 1-6-2011

Please cite this article as: Alcazar-Fuoli L, Cuesta I, Rodriguez-Tudela JL, Cuenca-Estrella M, Sanglard D, Mellado E, Three-dimensional models of 14α-sterol demethylase (Cyp51A) from *Aspergillus lentulus* and *Aspergillus fumigatus*: an insight into differences in voriconazole interaction, *International Journal of Antimicrobial Agents* (2010), doi:10.1016/j.ijantimicag.2011.06.005

Three-dimensional models of 14α-sterol demethylase (Cyp51A) from *Aspergillus lentulus* and *Aspergillus fumigatus*: an insight into differences in voriconazole interaction

Laura Alcazar-Fuoli [a,1,2], Isabel Cuesta [a,1], Juan L. Rodriguez-Tudela [a], Manuel Cuenca-Estrella [a], Dominique Sanglard [b], Emilia Mellado [a,*]

[a] *Mycology Reference Laboratory, Centro Nacional de Microbiologia, Instituto de Salud Carlos III, Carretera Majadahonda-Pozuelo Km 2, 28220 Madrid, Spain*

[b] *Institute of Microbiology, University of Lausanne and University Hospital Centre, Lausanne, Switzerland*

ARTICLE INFO

Article history:

Received 23 November 2010

Accepted 1 June 2011

Keywords:

Aspergillus spp.

Azole resistance

Cyp51A

3D models

* Corresponding author. Tel.: +34 918 223 427; fax: +34 915 097 919.

E-mail address: emellado@isciii.es (E. Mellado).

[1] These two authors contributed equally to this work

[2] Present address: Department of Microbiology, Imperial College London, Centre for Molecular Microbiology and Infection, Armstrong Road, London SW7 2AZ, UK.

ABSTRACT

Aspergillus lentulus, an *Aspergillus fumigatus* sibling species, is increasingly reported in corticosteroid-treated patients. Its clinical significance is unknown, but the fact that *A. lentulus* shows reduced antifungal susceptibility, mainly to voriconazole, is of serious concern. Heterologous expression of *cyp51A* from *A. fumigatus* and *A. lentulus* was performed in *Saccharomyces cerevisiae* to assess differences in the interaction of Cyp51A with the azole drugs. The absence of endogenous *ERG11* was efficiently complemented in *S. cerevisiae* by the expression of either *Aspergillus cyp51A* allele. There was a marked difference between azole minimum inhibitory concentration (MIC) values of the clones expressing each *Aspergillus* spp. *cyp51A*. *Saccharomyces cerevisiae* clones expressing *A. lentulus* alleles showed higher MICs to all of the azoles tested, supporting the hypothesis that the intrinsic azole resistance of *A. lentulus* could be associated with Cyp51A. Homology models of *A. fumigatus* and *A. lentulus* Cyp51A protein based on the crystal structure of Cyp51p from *Mycobacterium tuberculosis* in complex with fluconazole were almost identical owing to their mutual high sequence identity. Molecular dynamics (MD) was applied to both three-dimensional protein models to refine the homology modelling and to explore possible differences in the Cyp51A–voriconazole interaction. After 20 ns of MD modelling, some critical differences were observed in the putative closed form adopted by the protein upon voriconazole binding. A closer study of the *A. fumigatus* and *A. lentulus* voriconazole putative binding site in Cyp51A suggested that some major differences in the protein's BC loop could differentially affect the lock-up of voriconazole, which in turn could correlate with their different azole susceptibility profiles.

1. Introduction

Aspergillus fumigatus is the main causative agent of invasive aspergillosis, normally affecting immunocompromised patients suffering severe haematological malignancies and transplants recipients [1]. *Aspergillus fumigatus* belongs to the Fumigati section, where there are other species that are indistinguishable by means of classical identification methods. Within this complex, besides *A*. *fumigatus*, other species such as *Aspergillus lentulus*, *Neosartorya udagawae*, *Neosartorya pseudofischeri*, *Neosartorya hiratsukae* and *Aspergillus viridinutants* have been reported in human infections [2–9]. *Aspergillus lentulus* was first described in 2005, isolated from neutropenic patients with a fatal outcome [3]. Invasive infections by *A*. *lentulus* are rare, but this species has started to be reported in non-neutropenic patients receiving corticosteroid treatment and is also frequently isolated from respiratory samples [10–13].

Most *A*. *fumigatus* strains are susceptible to the antifungals commonly used for the treatment of invasive infections [14–16]. However, *A*. *fumigatus* strains with secondary resistance to azole drugs have been described and their resistance mechanism usually involves single mutations in the *cyp51A* gene [17–20]. On the other hand, to date all *A. lentulus* clinical isolates show high minimum inhibitory concentrations (MICs) to amphotericin B, echinocandins and azole drugs [12,21–23]. Among the azoles, *A. lentulus* strains are especially resistant to voriconazole (MICs > 4.0 mg/L) [12,21,22]. In contrast to *A*. *fumigatus,* this azole resistance could be considered intrinsic since all isolates exhibit similar azole resistance patterns [12,21].

The cytochrome P450 14α-sterol demethylase encoded by *cyp51A* is the target responsible for azole drug activity in *A*. *fumigatus* [24]. However, the interaction between azoles and Cyp51A has never been elucidated in *A*. *lentulus*. In this study, heterologous expression of *A*. *fumigatus* and *A*. *lentulus cyp51A* was first performed in a *Saccharomyces cerevisiae* strain in which the endogenous *ERG11* gene was conditionally expressed with a tetracycline-regulatable system [25–27]. Differences in the interaction of the azole drugs between both *Aspergillus* species were therefore assessed.

Next, three-dimensional (3D) Cyp51A theoretical models were performed in order to propose hypothetical differences in azole–target interaction within these two closely related *Aspergillus* species. Currently, all known forms of fungal Cyp51 are membrane-bound microsomal enzymes, thus complicating structural studies of this protein by X-ray crystallography. In the absence of a crystal structure of *A*. *fumigatus* Cyp51A, understanding the complexity of Cyp51 substrate/inhibitor binding and the involved conformational changes has relied on the use of homology models [28–30]. In this study, predicted *Aspergillus* Cyp51A 3D structures, based on the crystal structure of *Mycobacterium tuberculosis* Cyp51 ortholog, were used. Differences in voriconazole interaction between the Cyp51A enzymes from both *Aspergillus* species were explored by molecular docking and molecular dynamics (MD).

2. Material and methods

2.1. Strains and media

The *S. cerevisiae* strains used were: (i) DSY3886, derived from Y40122 [MAT**a***ura*3-52*leu*2Δ1*his*3Δ200GAL2CMVp(tetR'-SSN6)::LEU2*trp*1::Tta]; (ii) DSY3899, derived from DSY3886 but with *ERG11* under the control of doxycycline [MAT**a***ura*3-52*leu*2Δ1*his*3Δ200GAL2CMVp(tetR'SSN6)::LEU2*trp*1::TtaERG11::kanMX-tetO$_7$]; and (iii) DSY3961, derived from DSY3899 in which the ABC transporter *PDR5* was deleted to diminish the intrinsic low azole susceptibility of *S. cerevisiae* [MAT**a***ura*3-52*leu*2Δ1*his*3Δ200GAL2CMVp(tetR'SSN6)::LEU2*trp*1::TtaERG11::kanMXtetO$_7$*pdr5*Δ::HIS3kanMX] [27]. *Aspergillus fumigatus* CM237 and *A*. *lentulus* CM1290 strains were used to obtain Cyp51A cDNA. *Saccharomyces cerevisiae* and *Aspergillus* strains were grown as described previously [20,26].

2.2. Functional complementation

Aspergillus cyp51A cDNA flanked by pYES2/CT homologous regions was amplified by polymerase chain reaction (PCR) using primers Cy51F and Cy51R [27]. The vector pYES2/CT (Invitrogen, Lausanne, Switzerland) was *Hind*III/*Xho*I linearised prior to *S*. *cerevisiae* DSY3961 strain transformation with 5 μL of the digested plasmid and 5 μL of the *A*. *fumigatus* or *A*. *lentulus cyp51A* PCR products. Transformants were selected on minimal yeast nitrogen base medium without uracil (YNB–ura). Twenty transformants for each *Aspergillus* cDNA background were screened for *ERG11* functional complementation by growth in YNB–ura liquid medium and inoculating 4 μL of the yeast

cultures on YNB–ura agar plates containing galactose (2%), with and without doxycycline (2 μg/mL). *cyp51A* genes were amplified from transformed yeast and were then sequenced for verification. *Aspergillus fumigatus* primers aimed to the *cyp51A* amplification were used to amplify the *cyp51A* gene from *A. lentulus* [31]. The *A. lentulus cyp51A* gene was amplified and sequenced from ten *A. lentulus* strains and all of them had the same *cyp51A* sequence and the same azole susceptibility. Sequences were processed using Lasergene (DNASTAR Inc., Madison, WI). Oligonucleotides were purchased from Eurogentec S.A. (Liège, Belgium).

Protein extracts for immunoblotting were prepared by alkaline extraction from overnight cultures induced with galactose. Immunodetection was performed with a polyclonal mouse anti-His-tag antibody [26,32].

2.3. Etest susceptibility testing

Standardisation of growth conditions was performed prior to azole susceptibility testing of individual *S. cerevisiae* clones expressing each different *cyp51A* cDNA [26]. The clones were tested against fluconazole and voriconazole (Pfizer S.A., Madrid, Spain), itraconazole (Janssen Pharmaceutical S.A., Madrid, Spain) and posaconazole (Merck & Co, Madrid, Spain) grown in YNB–ura with galactose (2%) and doxycycline (2 μg/mL). The experiment was performed on at least three occasions and all values, converted to $\log_2$ values to achieve a normal distribution, were used for graphical representation. The significance of the differences in MICs was determined by Student's *t*-test. A *P*-value of <0.05 was considered significant.

2.4. Comparative models of cytochrome P450 14α-sterol demethylase (Cyp51A) proteins

Structural models of Cyp51A wild-type enzymes from *A*. *fumigatus* (*Af*Cyp51A) and *A*. *lentulus* (*Al*Cyp51A) strains were constructed by standard comparative modelling methods and the software DeepView [33]. The structure of Cyp51p from *M*. *tuberculosis* (*Mt*Cyp51p) in complex with fluconazole, deposited in the Protein Data Bank (PDB) [34] with code 1EA1 [35], was used as a template. The amino acid sequence identity of *Af*Cyp51A and *Al*Cyp51A with *Mt*Cyp51p was 26% and 27%, respectively. The alignment was then manually optimised on the basis of knowledge-based methods to avoid gap insertion where conserved secondary structure motifs were present. The N-terminal of *Aspergillus* spp. Cyp51A (residues 1–34) were assumed to comprise the membrane-spanning domains, thus with no counterparts in the template protein, and were deleted prior to protein modelling. Finally, a full prediction of the rest of the protein residues comprised within the homology profile defined by the template's sequence (all loops included) was rendered by the homology modelling method [33]. The quality of both protein models was checked using the analysis programs (Anolea, Gromos and Verify3D) provided by the SWISS-MODEL server [36–38]. [Available new structures, such as PDB:3LD6 and PDB:3JUV, show an average root mean square deviation (RMSD) of 1.50 Å to PDB:1EA1. From the point of view of the homology modelling procedure, all those experimental structures could also result in suitable templates, as global differences among them fall bellow crystallisation resolution values.]

2.5. Drug modelling and voriconazole docking

A model of the voriconazole drug was constructed de novo with Biomol-Informatics (http://www.biomol-informatics.com) software facilities, and its geometry was refined by means of the MOPAC7 [39] semi-empirical quantum mechanics methods and the AM1 Hamiltonian [40]. Electrostatic point charges at AM1 optimised geometry were calculated with bond charge correction at the same level. The heme–cysteine complex position in both *Aspergillus* spp. Cyp51A models was set by structural alignment with ligand overlapping. The initial docked location of voriconazole in Cyp51A models was set with AutoDock 4.0 software suite [41,42], preserving the conformation of the triazole and the difluorophenyl rings as in the fluconazole binding model reported in the PDB:1EA1 crystal structure.

2.6. Molecular mechanics force fields

Amber's ff99SB [43] force field from the same-name molecular dynamics (MD) software suite [44] was used for both Cyp51A protein models. Bonded and non-bonded parameters of voriconazole were assigned with the Antechamber modules as the General Amber Force Field [45] for chemical compounds. Contributed parameters for the heme group [46] in the AMBER10 distribution were modified and adapted by analogy with the ff99SB force field to model complexed cysteines.

2.7. Molecular dynamics simulations

All MD simulations were set up and performed using AMBER10. Each molecular system was composed of the corresponding model of the Cyp51A protein with its heme–cysteine complex and voriconazole, and was embedded in a truncated octahedron box of TIP3P water molecules, keeping a distance of 10 Å between the limits of the box and the closest atom of the solute. In order to neutralise the electrostatic charge of each system, potassium ions were also added. Periodic boundary conditions, the Amber's implementation of the particle mesh Ewald treatment of electrostatic interactions, a non-bonded cut-off distance of 8 Å and the SHAKE algorithm with an integration step of 2.0 fs were imposed in all MD calculations. Initial relaxation of each solvated complex was completed by performing 10 000 steps of energy minimisation, followed by 50 ps of constant volume MD equilibration run, raising the temperature progressively from 0 to 300 K while keeping mild harmonic restrains (5 Kcal·mol^{-1}·Å^{-2}). After relaxation of the Cyp51A complex, solvent and counter ions, another 50 ps MD were run to equilibrate the system at constant temperature (300 K) and pressure (1 atm), at the time that initial positional restraints were gradually removed. Finally, 20 ns of productive unrestrained MD were run. For each system, the average structure of the last nanosecond of MD was minimised and then selected as a representative model of Cyp51A bound to voriconazole in *A. fumigatus* or *A. lentulus*. RMSD values during MD simulation were monitored both for the whole protein structure and for the BC loop of the two proteins bound to voriconazole (Supplementary Fig. 1).

2.8. GenBank accession numbers

The *cyp51A* sequences have been deposited in GenBank as AF338659 (*A*. *fumigatus*) and GU479991 (*A*. *lentulus*).

3. Results

3.1. cyp51A functional complementation in Saccharomyces cerevisiae

The *cyp51A* functional complementation was performed by conditional expression of the yeast *ERG11* gene with a tetracycline-regulatable system [27,47] and induced expression of *cyp51A* cDNA from *A*. *fumigatus* and *A*. *lentulus* under the control of the *GAL1* promoter in *S*. *cerevisiae*. The lack of *ERG11* was efficiently complemented by the expression of either *Aspergillus cyp51A* allele under selective conditions (Fig. 1A). No growth in doxycycline selective medium was observed when DSY3961 strain was not complemented with any *Aspergillus* cDNA (data not shown). Two clones growing in doxycycline-containing medium were analysed by Western blot to verify the Cyp51A protein expression (Fig. 1B).

All *cyp51A* sequences were identical to *A*. *fumigatus* or *A*. *lentulus cyp51A* sequences, respectively, with the exception of one clone for DSY3961+CM1290cDNA that exhibited nucleotide changes compared with the original CM1290 *cyp51A*. This resulted in non-synonymous changes but on a non-conserved region of the Cyp51A protein (K153E, D253N, T289A and Q418R). These two clones were analysed independently and named as DSY3961+CM1290cDNA (a) and (b).

3.2. Azole drug susceptibility

Two *S. cerevisiae* clones for every *Aspergillus* spp. *cyp51A* allele were chosen for azole susceptibility analysis by Etest. All clones expressing *Aspergillus* spp. *cyp51A* showed higher MICs to fluconazole compared with the *S. cerevisiae* background strain (data not shown). This is consistent with the intrinsic fluconazole resistance shown by *Aspergillus* spp*. Saccharomyces cerevisiae* clones expressing *A. lentulus cyp51A* alleles showed higher MICs to itraconazole, posaconazole and voriconazole than those expressing *A. fumigatus cyp51A* alleles (Fig. 1C). Differences in azole susceptibilities were observed between clones with the same *A. lentulus* cDNA background [DSY3961+CM1290cDNA (b) showed higher MICs than DSY3961+CM1290cDNA (a); Fig. 1C]. These differences could be due either to the nucleotide changes that were found in DSY3961+CM1290cDNA (b) or to an increase in *cyp51A* expression depending on the plasmid copy number. However, statistical analysis showed that despite the slight difference between CM1290 clones, the expression of both *cyp51A* cDNA variants resulted in increased resistance to all azoles tested compared with *A. fumigatus*.

3.3. Aspergillus fumigatus and Aspergillus lentulus Cyp51A three-dimensional protein homology modelling

A 3D homology model was constructed to explore possible structural differences in voriconazole interaction between Cyp51A from *A*. *fumigatus* (*Af*Cyp51A) and *A*. *lentulus* (*Al*Cyp51A). The crystal structure of 14α-sterol demethylase from *M*. *tuberculosis*

(*Mt*Cyp51p) in complex with fluconazole (PDB code:1EA1) provided the common template for the modelling and posterior differential study of these eukaryotic orthologs of *Aspergillus* Cyp51A proteins (sequence identity between *Al*Cyp51A and *Af*Cyp51A proteins is 95%) (Fig. 2). 3D modelled structures of Cyp51A in *A. fumigatus* and *A. lentulus* showed an overall structural similarity to the structural template of 1.98Å and 1.81Å, in terms of RMSD of their respective Cα backbone traces (Fig. 3). No clear differences in the putative voriconazole binding site could be deduced from comparison of mere homology modelling-obtained structures. The few different residues between the two proteins lay outside the theoretical substrate recognition site (Fig. 2). To obtain a better adjustment of the structures, the hypothetical models of both proteins were subject to a standard MD protocol.

3.4. Docking of the inhibitor into the catalytic site: insights into voriconazole binding

To detect possible critical differences arising from both theoretical models, the structure–activity relationship of voriconazole was examined based on the docking models and subsequent unrestrained MD simulation for 20 ns. After the MD, voriconazole's putative internal conformation within the bound form of Cyp51A was essentially identical in *A. fumigatus* and *A. lentulus.* It could become partially stabilised by the formation of the complex voriconazole–heme–Cyp51A through the triazolyl group, and by an internal hydrogen-bonded interaction between the hydroxyl group and the nitrogen N1 in the 5-fluoropyrimidinyl moiety. This result indicates that the dynamics did not affect the inhibitor basic positioning inside the active site of the protein. However, the structural predictions obtained after 20 ns of unrestrained MD suggest that a different structure for

the BC loop is reached after voriconazole binding. The BC loop [33,50] is situated between the α-helixes B and C and covers the protein region that ranges between residues 96 and 127 in *A*. *fumigatus* and *A*. *lentulus* models (Fig. 2). Despite the total BC loop sequence conservation between both Cyp51A enzymes, the dissimilar conformation around voriconazole could be putatively related to their differential susceptibility to the inhibitor (Fig. 4; Supplementary Fig. 1). The model for *Af*Cyp51A BC loop conformation shows that the occlusion of the catalytic centre upon voriconazole binding could be mediated by the residues Y107, L110, F115 and F134 with the azole. On the other hand, the more relaxed *Al*Cyp51A BC loop structure would behave differently with respect to azole interactions since the residues 4 Å around voriconazole are Y107, L110 and T111 and V114. For this reason, in *Al*Cyp51A a tandem of three aromatic residues of tyrosine and phenylalanine would not participate in voriconazole stabilisation, likely resulting in a weaker interaction in comparison with *Af*Cyp51A (Fig. 5).

4. Discussion

Resistance to antifungals is a recognised problem that occurs at low frequency, but with increasing rates in some countries [18,51,52]. As voriconazole is the recommended treatment for invasive aspergillosis, the increasing incidence of azole resistance represents a real concern. Few surveillance studies have been carried out to date [11], therefore similar resistance rates may exist in other countries. In *A. fumigatus*, drug resistance is largely confined to the azole class drugs, whilst resistance to polyene or echinocandin drugs is uncommon. However, as the number of patients with disease or

chemically-induced immune deficiencies increases, resistance among clinical strains may became more common, especially with the expanded use of second-generation triazole drugs for prophylaxis and empirical therapy. Moreover, resistance to antifungal agents may be intrinsically present and the recent changes in the taxonomy of *Aspergillus* spp. have implications on the interpretation of drug susceptibility profiles [53]. For example, *A. lentulus* antifungal susceptibility testing indicated that this species is less susceptible to azole antifungals than *A. fumigatus* [12,21,22]. Moreover, this decreased azole susceptibility appears to be intrinsic since all strains behaved in a similar manner [21].

In this work, functional complementation of the essential gene *ERG11* from *S. cerevisiae* was accomplished by heterologous expression of *A. fumigatus* and *A. lentulus cyp51A* alleles. Differences in azole susceptibility of clones bearing *cyp51A* alleles with different point mutations, known to be responsible for azole resistance, have been addressed previously [27]. A similar functional complementation system was recently used to demonstrate *A. fumigatus* Cyp51A and Cyp51B function as 14α-sterol demethylases in ergosterol biosynthesis [54]. Moreover, confirmation of the role of Cyp51A in the intrinsic resistance of *A. fumigatus* to fluconazole has been demonstrated [27,54]. Reduced susceptibility of *A. lentulus* to azoles is supported by the results of the current study as *S. cerevisiae* strains expressing *A. lentulus cyp51A* cDNA were significantly less susceptible to all azole drugs than those expressing *A. fumigatus cyp51A* (Fig. 1C). Although one of the clones harboured some point mutations responsible for amino acid changes, all of the amino acids are present in other Cyp51A enzymes from azole-

susceptible fungal species. Therefore, the differences found in the MIC values between clones are more likely due to the variable copy number of the plasmid.

The *A*. *fumigatus* and *A*. *lentulus* Cyp51Ap sequences are 95% identical. Since the few amino acid changes could not explain, a priori, the differences in azole susceptibility, the next step was an analysis of the structural conformation of these closely related proteins. No crystal structure of Cyp51 from fungi has yet been obtained, probably because they are membrane proteins that are difficult to purify and crystallise under current conditions [55]. In the absence of a crystal structure, computer-assisted homology modelling was used to predict the 3D structures of *Af*Cyp51A and *Al*Cyp51A and to determine the structural basis for the differences in their voriconazole affinity. The crystal structure of *M*. *tuberculosis* Cyp51p (*Mt*Cyp51p) that has been solved bound to fluconazole and 4-phenylimidazole was used [35]. Despite a lack of overall sequence identity, *Mt*Cyp51p shares conserved substrate recognition site motifs and structure with its mammalian, plant and fungal orthologs [48]. Homology models have been previously used to flag up possible protein–drug interactions by providing an insight into which residues in Cyp51 appear to be important for ligand binding [56]. In fact, Cyp51 homology models, based on prokaryotic P450s, have been reported for *Candida albicans*, *Candida krusei* and *S*. *cerevisiae* [57–61]. Currently, the *M*. *tuberculosis* Cyp51p is being used as a template in models for fungal Cyp51 enzymes such as *Penicillium digitatum, C*. *albicans*, *A*. *fumigatus* and *Cryptococcus neoformans* [28,55,56]. Moreover, several models have been previously inferred for *A*. *fumigatus* Cyp51A in combination with itraconazole, voriconazole and posaconazole, providing predictions about how the different azoles interact with *Af*Cyp51A [28–30].

The 3D folding patterns of the overall superimposed *Af*Cyp51A and *Al*Cyp51A structures were very similar. Also, voriconazole's internal conformation within the bound form of Cyp51A derived from docking models was essentially identical in *A*. *fumigatus* and *A*. *lentulus*. Both the *Af*Cyp51A and *Al*Cyp51A models have a substrate access channel embedded in the interior of the protein, sharing similar topological features to those in *Mt*Cyp51p [28]. In the crystal structure of *Mt*Cyp51p, the N-terminus of the I helix and the BC loop form the entrance of the substrate access channel. The I helix has a potential ability to bend in response to certain stimuli, such as substrate or redox partner binding, to release the BC loop from close contacts in the binding site, enlarging the space available for substrate or inhibitor binding [28,35].

Despite the total *Af*Cyp51A and *Al*Cyp51A BC loop sequence conservation, the MD simulation supports the hypothesis that their closed conformation around voriconazole could be putatively related to their differential susceptibility to the inhibitor. Therefore, the BC loop conformation in the *A*. *fumigatus* model would allow the catalytic site to remain occluded upon the triazole derivative binding and so stabilises the voriconazole–heme–C454 coordination complex in a closed configuration. However, the *A*. *lentulus* BC loop could not perform such a task, possibly due to the alternative position reached by this region after binding of the inhibitor, as suggested by the MD simulation. The experimentally detected differential behaviour of both systems towards voriconazole could be a direct consequence of different contact patterns among protein residues, the inhibitor and the heme group at this site. The model for *A*. *fumigatus* BC loop conformation shows that occlusion of the catalytic centre upon voriconazole binding

appears to be mediated by the residues Y107, L110, F115 and F134 with the azole. In a previous *Af*Cyp51 model [28], F115 was one of the residues in the substrate access channel sited in the B' helix inside the BC loop. Moreover, F134 and Y107 form part of the hydrophobic cleft that interacts with the substrate and stabilises it in the active site [28]. The differences found in the location of the *Al*Cyp51A residues at 4 Å around voriconazole (Y107, L110 and T111 and V114) would explain a different voriconazole–Cyp51A interaction owing to the lack of a tandem of three aromatic residues and would not allow for efficient voriconazole stabilisation like that seen with *Af*Cyp51A. Moreover, the recent description that non-synonymous amino acids alterations in an *A. fumigatus* Cyp51A homology model, located far from the two ligand access channels and outside of the conserved regions of the Cyp51A protein, do not affect Cyp51A biological activity may support these argument [30].

Xiao et al. [29] have previously defined that aromatic and hydrophobic interactions are the primary binding determinants between voriconazole and residues Y107, F115, M292, A293, I364, I367 and L494. In agreement with this finding, Sheng et al. [55] using the *C*. *neoformans* Cyp51 model showed that the higher affinity of voriconazole for the protein may be due to an extra hydrophobic interaction with the phenyl group of Y131. Moreover, substitutions in the regions surrounding residue F134 have also been related to voriconazole resistance shown by *Absidia corymbifera* and *Rhizopus oryzae* [62].

In summary, the data presented here indicate that *A*. *lentulus* is less susceptible to all azole drugs. The reduced susceptibility to voriconazole shown by *A*. *lentulus* appears to be due to a decreased affinity of the target Cyp51A for this azole, as deduced indirectly

from susceptibility patterns in *S. cerevisiae.* However, further insights into the azole drug interaction of Cyp51A are still speculative until a crystal structure is available. Meanwhile, the study of molecular mechanisms of antifungal drug resistance is important in order to understand better the basis of resistance and to develop clinical and pharmacological strategies to avoid resistance in the future. The structural model of *A. lentulus* Cyp51A described in this study can be used in azole drug optimisation, virtual screening or de novo inhibitor synthesis to improve the treatment of infections caused by this intrinsically azole-resistant species of fungi [63,64]. In addition, the knowledge of enzyme–inhibitor interactions would be useful in developing new, or more potent, antifungal drugs.

Acknowledgments

The authors thank Biomol-Informatics S.L. (http://www.biomol-informatics.com) for bioinformatics consulting.

Funding

This work was supported by the Ministerio de Ciencia e Innovación (MICINN) (grant no. SAF2008-04143) as well as by European Union funding under an EU-STREP project (LSHM-CT-2005-518199; acronym EURESFUN). IC has a research contract with the Fondo de Investigación Sanitario at Instituto de Salud Carlos III (REIPI) (project MPY 1022/07).

Competing interests

EM, LA-F, IC and DS report no conflict of interest that could influence or bias the results of the present work. EM has been paid for a talk on behalf of Gilead Sciences in October 2010. In the past 5 years, MC-E has received grant support from Astellas Pharma, bioMérieux, Gilead Sciences, Merck Sharp and Dohme (MSD), Pfizer, Schering-Plough, Soria Melguizo SA, the European Union, the ALBAN program, the Spanish Agency for International Cooperation, the Spanish Ministry of Culture and Education, the Spanish Health Research Fund, the Instituto de Salud Carlos III, The Ramón Areces Foundation and The Mutua Madrileña Foundation; he has been advisor/consultant to the Pan American Health Organization, Gilead Sciences, MSD, Pfizer and Schering-Plough and has been paid for on behalf of Gilead Sciences, MSD, Pfizer and Schering-Plough. In the past 5 years, JLR-T has received grant support from Astellas Pharma, Gilead Sciences, MSD, Pfizer, Schering-Plough, Soria Melguizo SA, the European Union, the Spanish Agency for International Cooperation, the Spanish Ministry of Culture and Education, the Spanish Health Research Fund, the Instituto de Salud Carlos III, The Ramón Areces Foundation and The Mutua Madrileña Foundation; he has been an advisor/consultant to the Pan American Health Organization, Gilead Sciences, MSD, Myconostica, Pfizer and Schering -Plough and has been paid for talks on behalf of Gilead Sciences, MDS, Pfizer and Schering-Plough.

Ethical approval

Not required.

References

[1] Segal BH. Aspergillosis. N Engl J Med 2009;360:1870–84.

[2] Balajee SA, Gribskov JL, Brandt M, Ito J, Fothergill A, Marr KA. Mistaken identity: *Neosartorya pseudofischeri* and its anamorph masquerading as *Aspergillus fumigatus*. J Clin Microbiol 2005;43:5996–9.

[3] Balajee SA, Gribskov JL, Hanley E, Nickle D, Marr KA. *Aspergillus lentulus* sp. nov., a new sibling species of *A*. *fumigatus*. Eukaryot Cell 2005;4:625–32.

[4] Ghebremedhin B, Bluemel A, Neumann KH, Koenig B, Koenig W. Peritonitis due to *Neosartorya pseudofischeri* in an elderly patient undergoing peritoneal dialysis successfully treated with voriconazole. J Med Microbiol 2009;58:678–82.

[5] Koutroutsos K, Arabatzis M, Bougatsos G, Xanthaki A, Toutouza M, Velegraki A. *Neosartorya hiratsukae* peritonitis through continuous ambulatory peritoneal dialysis. J Med Microbiol 2010;59:862–5.

[6] Guarro J, Kallas EG, Godoy P, Karenina A, Gene J, Stchigel A, et al. Cerebral aspergillosis caused by *Neosartorya hiratsukae*, Brazil. Emerg Infect Dis 2002;8:989–91.

[7] Jarv H, Lehtmaa J, Summerbell RC, Hoekstra ES, Samson RA, Naaber P. Isolation of *Neosartorya pseudofischeri* from blood: first hint of pulmonary aspergillosis. J Clin Microbiol 2004;42:925–8.

[8] Vinh DC, Shea YR, Jones PA, Freeman AF, Zelazny A, Holland SM. Chronic invasive aspergillosis caused by *Aspergillus viridinutans*. Emerg Infect Dis 2009;15:1292–4.

[9] Vinh DC, Shea YR, Sugui JA, Parrilla-Castellar ER, Freeman AF, Campbell JW, et al. Invasive aspergillosis due to *Neosartorya udagawae*. Clin Infect Dis 2009;49:102–11.

[10] Alhambra A, Catalán M, Moragues MD, Brena S, Ponton J, Montejo JC, et al. Isolation of *Aspergillus lentulus* in Spain from a critically ill patient with chronic obstructive pulmonary disease. Rev Iberoam Micol 2008;25:246–9.

[11] Balajee SA, Kano R, Baddley JW, Moser SA, Marr KA, Alexander BD, et al. Molecular identification of *Aspergillus* species collected for the Transplant-Associated Infection Surveillance Network. J Clin Microbiol 2009;47:3138–41.

[12] Mellado E, Alcazar-Fuoli L, García-Effrón G, Alastruey-Izquierdo A, Cuenca-Estrella M, Rodriguez-Tudela JL. New resistance mechanisms to azole drugs in *Aspergillus fumigatus* and emergence of antifungal drugs-resistant *A*. *fumigatus* atypical strains. Med Mycol 2006;44:S367–71.

[13] Montenegro G, Sánchez Puch S, Jewtuchowicz VM, Pinoni MV, Relloso S, Temporitti E, et al. Phenotypic and genotypic characterization of *Aspergillus lentulus* and *Aspergillus fumigatus* isolates in a patient with probable invasive aspergillosis. J Med Microbiol 2009;58:391–5.

[14] Cuenca-Estrella M, Gomez-Lopez A, Mellado E, Buitrago MJ, Monzón A, Rodriguez-Tudela JL. A head-to-head comparison of currently available antifungal agents for 3,378 Spanish clinical isolates of yeasts and filamentous fungi. Antimicrob Agents Chemother 2006;50:917–21.

[15] Gomez-Lopez A, Garcia-Effron G, Mellado E, Monzon A, Rodriguez-Tudela JL, Cuenca-Estrella M. In vitro activities of three licensed antifungal agents against

Spanish clinical isolates of *Aspergillus* spp. Antimicrob Agents Chemother 2003;47:3085–8.

[16] Rodriguez-Tudela JL, Alcazar-Fuoli L, Mellado E, Alastruey-Izquierdo A, Monzon A, Cuenca-Estrella M. Epidemiological cutoffs and cross-resistance to azole drugs in *Aspergillus fumigatus*. Antimicrob Agents Chemother 2008;52:2468–72.

[17] Diaz-Guerra TM, Mellado E, Cuenca-Estrella M, Rodriguez-Tudela JL. A point mutation in the 14α-sterol demethylase gene *cyp51A* contributes to itraconazole resistance in *Aspergillus fumigatus*. Antimicrob Agents Chemother 2003;47:1120–4.

[18] Howard SJ, Cerar D, Anderson MJ, Albarrag A, Fisher MC, Pasqualotto AC, et al. Frequency and evolution of azole resistance in *Aspergillus fumigatus* associated with treatment failure. Emerg Infect Dis 2009;15:1068–76.

[19] Mellado E, Garcia-Effron G, Alcazar-Fuoli L, Cuenca-Estrella M, Rodriguez-Tudela JL. Substitutions at methionine 220 in the 14α-sterol demethylase (Cyp51A) of *Aspergillus fumigatus* are responsible for resistance in vitro to azole antifungal drugs. Antimicrob Agents Chemother 2004;48:2747–50.

[20] Mellado E, Garcia-Effron G, Alcazar-Fuoli L, Melchers WJ, Verweij PE, Cuenca-Estrella M, et al. A new *Aspergillus fumigatus* resistance mechanism conferring in vitro cross-resistance to azole antifungals involves a combination of *cyp51A* alterations. Antimicrob Agents Chemother 2007;51:1897–904.

[21] Alcazar-Fuoli L, Mellado E, Alastruey-Izquierdo A, Cuenca-Estrella M, Rodriguez-Tudela JL. *Aspergillus* section Fumigati: antifungal susceptibility patterns and sequence-based identification. Antimicrob Agents Chemother 2008;52:1244–51.

[22] Balajee, SA, Weaver M, Imhof A, Gribskov J, Marr KA. *Aspergillus fumigatus* variant with decreased susceptibility to multiple antifungals. Antimicrob Agents Chemother 2004;48:1197–203.

[23] Staab, JF, Kahn JN, Marr KA. Differential *Aspergillus lentulus* echinocandin susceptibilities are Fksp independent. Antimicrob Agents Chemother 2010;54:4992–8.

[24] Mellado E, Garcia-Effron G, Buitrago MJ, Alcazar-Fuoli L, Cuenca-Estrella M, Rodriguez-Tudela JL. Targeted gene disruption of the 14-α sterol demethylase (*cyp51A*) in *Aspergillus fumigatus* and its role in azole drug susceptibility. Antimicrob Agents Chemother 2005;49:2536–8.

[25] Bellí G, Garí E, Aldea M, Herrero E. Functional analysis of yeast essential genes using a promoter-substitution cassette and the tetracycline-regulatable dual expression system. Yeast 1998;14:1127–38.

[26] Yen K, Gitsham P, Wishart J, Oliver SG, Zhang N. An improved *tet*O promoter replacement system for regulating the expression of yeast genes. Yeast 2003;20:1255–62.

[27] Alcazar-Fuoli L, Mellado E, Cuenca-Estrella M, Sanglard D. Probing the role of point mutations in the *cyp*51A gene from *Aspergillus fumigatus* in the model yeast *Saccharomyces cerevisiae*. Med Mycol 2010;49:276–84.

[28] Sheng CH, Zhang W, Zhang M, Song Y, Ji H, Yao J, et al. Homology modeling of lanosterol 14α-demethylase of *Candida albicans* and *Aspergillus fumigatus:* an insights into the enzyme–substrate interactions. J Biomol Struct Dyn 2004;22:91–9.

[29] Xiao L, Madison V, Chau AS, Loebenberg D, Palermo RE, McNicholas PM. Three-dimensional models of wild-type and mutated forms of cytochrome P450 14α-sterol demethylases from *Aspergillus fumigatus* and *Candida albicans* provide insights into posaconazole binding. Antimicrob Agents Chemother 2004;48:568–74.

[30] Snelders E, Karawajczyk A, Schaftenaar G, Verweij PE, Melchers WJ. Azole resistance profile of amino acid changes in *Aspergillus fumigatus* CYP51A based on protein homology modelling. Antimicrob Agents Chemother 2010;54:2425–30.

[31] Mellado E, Diaz-Guerra TM, Cuenca-Estrella M, Rodriguez-Tudela JL. Identification of two different 14-α sterol demethylase-related genes (*cyp51A* and *cyp51B*) in *Aspergillus fumigatus* and other *Aspergillus* species. J Clin Microbiol 2001;39:2431–8.

[32] Coste AT, Ramsdale M, Ischer F, Sanglard D. Divergent functions of three *Candida albicans* zinc-cluster transcription factors (CTA4, ASG1 and CTF1) complementing pleiotropic drug resistance in *Saccharomyces cerevisiae.* Microbiology 2008;154:1491–501.

[33] Guex N, Peitsch MC. SWISS-MODEL and the Swiss-PdbViewer: an environment for comparative protein modeling. Electrophoresis 1997;18:2714–23.

[34] Berman HM, Westbrook J, Feng Z, Gilliland G, Bhat TN, Weissig H, et al. The Protein Data Bank. Nucleic Acids Res 2000;28:235–42.

[35] Podust LM, Poulos TL, Waterman MR. Crystal structure of cytochrome P450 14α-sterol demethylase (CYP51) from *Mycobacterium tuberculosis* in complex with azole inhibitors. Proc Natl Acad Sci U S A 2001;98:3068–73.

[36] Guex N, Diemand A, Peitsch MC. Protein modelling for all. Trends Biochem Sci 1999;24:364–7.

[37] Peitsch MC. ProMod and Swiss-Model: Internet-based tools for automated comparative protein modelling. Biochem Soc Trans 1996;24:274–9.

[38] Schwede T, Kopp J, Guex N, Peitsch MC. SWISS-MODEL: an automated protein homology-modeling server. Nucleic Acids Res 2003;31:3381–5.

[39] Stewart JJ. MOPAC: a semiempirical molecular orbital program. J Comput Aided Mol Des 1990;4:1–105.

[40] Dewar MJS, Zoebisch EG, Healy EF, Stewart JJP. A new general purpose quantum mechanical molecular model. J Am Chem Soc 1985;107:3902–9.

[41] Huey R, Goodsell DS, Morris GM, Olson AJ. Grid-base hydrogen bond potentials with improved directionality. Lett Drug Des Discov 2004;1:178–83.

[42] Huey R, Morris GM, Olson AJ, Goodsell DS. A semiempirical free energy force field with charge-based desolvation. J Comput Chem 2007;28:1145–52.

[43] Hornak V, Abel R, Okur A, Strockbine B, Roitberg A, Simmerling C. Comparison of multiple Amber force fields and development of improved protein backbone parameters. Proteins 2006;65:712–25.

[44] Case DA, Darden TA, Cheatham III TE, Simmerling CL, Wang J, Duke RE, et al. *Assisted Model Building with Energy Refinement. AMBER 10*. San Francisco, CA: University of California; 2008.

[45] Wang J, Wolf RM, Caldwell JW, Kollman PA, Case DA. Development and testing of a general Amber force field. J Comput Chem 2004;25:1157–74.

[46] Giammona DA. An examination of conformational flexibility in porphyrin and bulky-ligand binding in myoglobin [PhD thesis]. Davis, CA: University of California, Davis; 1984.

[47] Wishart JA, Osborn M, Gent ME, Yen K, Vujovic Z, Gitsham P, et al. The relative merits of the *tet*O2 and *tet*O7 promoter systems for the functional analysis of heterologous genes in yeast and a compilation of essential yeast genes with *tet*O2 promoter substitutions. Yeast 2006;23:325–31.

[48] Lepesheva GI, Virus C, Waterman MR. Conservation in the CYP51 family. Role of the B' helix/BC loop and helices F and G in enzymatic function. Biochemistry 2003;42:9091–101.

[49] Snelders E, van der Lee HA, Kuijpers J, Rijs AJ, Varga J, Samson RA, et al. Emergence of azole resistance in *Aspergillus fumigatus* and spread of a single resistance mechanism. PLoS Med 2008;5:e219.

[50] Bueid A, Howard SJ, Moore CB, Richardson MD, Harrison E, Bowyer P, et al. Azole antifungal resistance in *Aspergillus fumigatus*: 2008 and 2009. J Antimicrob Chemother 2010;65:2116–8.

[51] van der Linden JWM, Warris A, Verweij PE. *Aspergillus* species intrinsically resistant to antifungal agents. Med Mycol 2011;49(Suppl 1):S82–9.

[52] Martel CM, Parker JE, Warrilow AG, Rolley NJ, Kelly SL, Kelly DE. Complementation of a *Saccharomyces cerevisiae* ERG11/CYP51 (sterol 14-α demethylase) doxycycline-regulated mutant and screening of the azole sensitivity of *Aspergillus fumigatus* isoenzymes CYP51A and CYP51B. Antimicrob Agents Chemother 2010;54:4920–3.

[53] Sheng Ch, Miao Z, Ji H, Yao J, Wang W, Che X, et al. Three-dimensional model of lanosterol 14α-demethylase from *Cryptococcus neoformans*: active-site characterization and insights into azole binding. Antimicrob Agents Chemother 2009;53:3487–95.

[54] Podust LM, Stojan J, Poulos TL, Waterman MR. Substrate recognition sites in 14α-sterol demethylase from comparative analysis of amino acid sequences and X-ray structure of *Mycobacterium tuberculosis* CYP51. J Inorg Biochem 2001;87:227–35.

[55] Zhao L, Liu D, Zhang Q, Zhang S, Wan J, Xiao WE. Expression and homology modeling of sterol 14α-demethylase from *Penicillium digitatum*. FEMS Microbiol Lett 2007:277:37–43.

[56] Boscott PE, Grant GH. Modeling cytochrome P450 14α-demethylase (*Candida albicans*) from P450cam. J Mol Graph 1994;12:185–92.

[57] Fukuoka T, Johnston DA, Winslow CA, de Groot MJ, Burt C, Hitchcock CA, et al. Genetic basis for differential activities of fluconazole and voriconazole against *Candida krusei*. Antimicrob Agents Chemother 2003;47:1213–9.

[58] Ji H, Zhang W, Zhou Y, Zhang M, Zhu J, Song Y, et al. A three-dimensional model of lanosterol 14α-demethylase of *Candida albicans* and its interaction with azole antifungals. J Med Chem 2000;43:2493–505.

[59] Morris G, Richards G. Molecular modelling of the sterol C-14 demethylase of *Saccharomyces cerevisiae*. Biochem Soc Trans 1991;19:793–5.

[60] Li H, Poulos TL. The structure of the cytochrome p450BM-3 haem domain complexed with the fatty acid substrate, palmitoleic acid. Nat Struct Biol 1997;4:140–6.

[61] Chau AS, Chen G, McNicholas PM, Mann PA. Molecular basis for enhanced activity of posaconazole against *Absidia corymbifera* and *Rhizopus oryzae.* Antimicrob Agents Chemother 2006;50:3917–9.

[62] Chai X, Zhang J, Hu H, Yu S, Sun Q, Dan Z, et al. Design, synthesis, and biological evaluation of novel triazole derivatives as inhibitors of cytochrome P450 14α-demethylase. Eur J Med Chem 2009;44:1913–20.

[63] Ruge E, Korting HC, Borelli C. Current state of three-dimensional characterisation of antifungal targets and its use for molecular modelling in drug design. Int J Antimicrob Agents 2005;26:427–41.

[64] Gouet P, Courcelle E, Stuart DI, Metoz F. ESPript: multiple sequence alignments in PostScript. Bioinformatics 1999;15:305–8.

Fig. 1. (A) Screening of clones *Saccharomyces cerevisiae* DSY3961+CM237cDNA and DSY3961+CM1290cDNA on minimal yeast nitrogen base medium without uracil (YNB–ura) in the presence of galactose (2%) with or without doxycycline (2 μg/ml). (B) Immunodetection of Cyp51A proteins for DSY3961+CM237cDNA (lane 1) and DSY3961+CM1290cDNA clones (a) and (b) (lanes 2 and 3). Lane 4, negative control (DSY3961+vector pYES2/CT). (C) Plots representing Etest susceptibility testing to itraconazole (white), voriconazole (grey) and posaconazole (black) for DSY3961+CM237cDNA, DSY3961+CM1290cDNA(a) and DSY3961+CM1290cDNA(b). *P*-values between *Aspergillus fumigatus* and *Aspergillus lentulus* clones are also shown. See Sections 2.1 and 3.1 for a description of the strains.

Fig. 2. Sequence alignment of amino acid sequences of *Aspergillus fumigatus*, *Aspergillus lentulus* and *Mycobacterium tuberculosis* Cyp51. Identical and similar residues are shown on a black background and with black frames, respectively. Asterisks mark the residues positioned <4 Å from voriconazole. The putative substrate binding site (black triangles) and the secondary structure elements of *M. tuberculosis* Cyp51p (PDB:1EA1) are labelled in agreement with the nomenclature of Podust et al. [48] using ESPript 2.2 [49].

Fig. 3. (A) Structural alignment of *Aspergillus fumigatus* (blue) and *Aspergillus lentulus* (yellow) protein three-dimensional (3D) models showing the putative conformation of a docked molecule of voriconazole (purple) within the catalytic site. (B) Details of docked

conformations of voriconazole to *A. fumigatus* (left) and *A. lentulus* (right) catalytic sites in the Cyp51 proteins.

Fig. 4. Surface representation of (A) *Aspergillus fumigatus* and (B) *Aspergillus lentulus* Cyp51A protein models after molecular dynamics (MD) simulation. Van der Waals atomic surface representation of *A. fumigatus* (A, light blue) and *A. lentulus* (B, light yellow) protein models as calculated from their respective theoretical structures bound to voriconazole and heme cofactor after 20 ns of MD. In (A), the *A. fumigatus* BC loop conformation (orange) almost completely occluding the access channel to the catalytic site of Cyp51A. In (B), the homologous BC loop of *A. lentulus* (red) leaving the voriconazole binding site basically accessible to the solvent. Protein surface in contact with voriconazole (purple) and the heme cofactor (green) are also shown.

Fig. 5. Representation of the modelled BC loop and contacting residues (Y107, F115 and F134) in (A) *Aspergillus fumigatus* and (B) *Aspergillus lentulus* Cyp51A catalytic centres after molecular dynamics simulation. The voriconazole molecule is coloured in purple and the heme cofactor in green.

Supplementary Fig. 1. Root mean square deviation (RMSD) from two molecular dynamics (MD) simulations of (A) *Aspergillus fumigatus* and (B) *Aspergillus lentulus* CYP51 models bound to voriconazole. CYP51 whole protein (red) and BC loop (black) backbone traces RMSD values are plotted in each panel. All values were calculated along a single 20 ns MD trajectory for each organism's model, taking as reference structure their respective comparative models based on CYP51 in complex with azole inhibitors from *Mycobacterium tuberculosis* (PDB:1EA1). In terms of RMSD, the whole backbone structure changes similarly in both models and remains stabilised during the last nanoseconds of simulation (red lines). In contrast, whilst the structure of the BC loop in *A. fumigatus* varies in a similar amount to the whole protein structure during the MD simulation (black line, upper panel), the same loop in *A. lentulus* (black line, lower panel) exhibits a more pronounced movement (RMSD values higher than 6 Å) that results in the differentiated open position of the *A. lentulus* BC loop showed as shown in Figs 4 and 5.

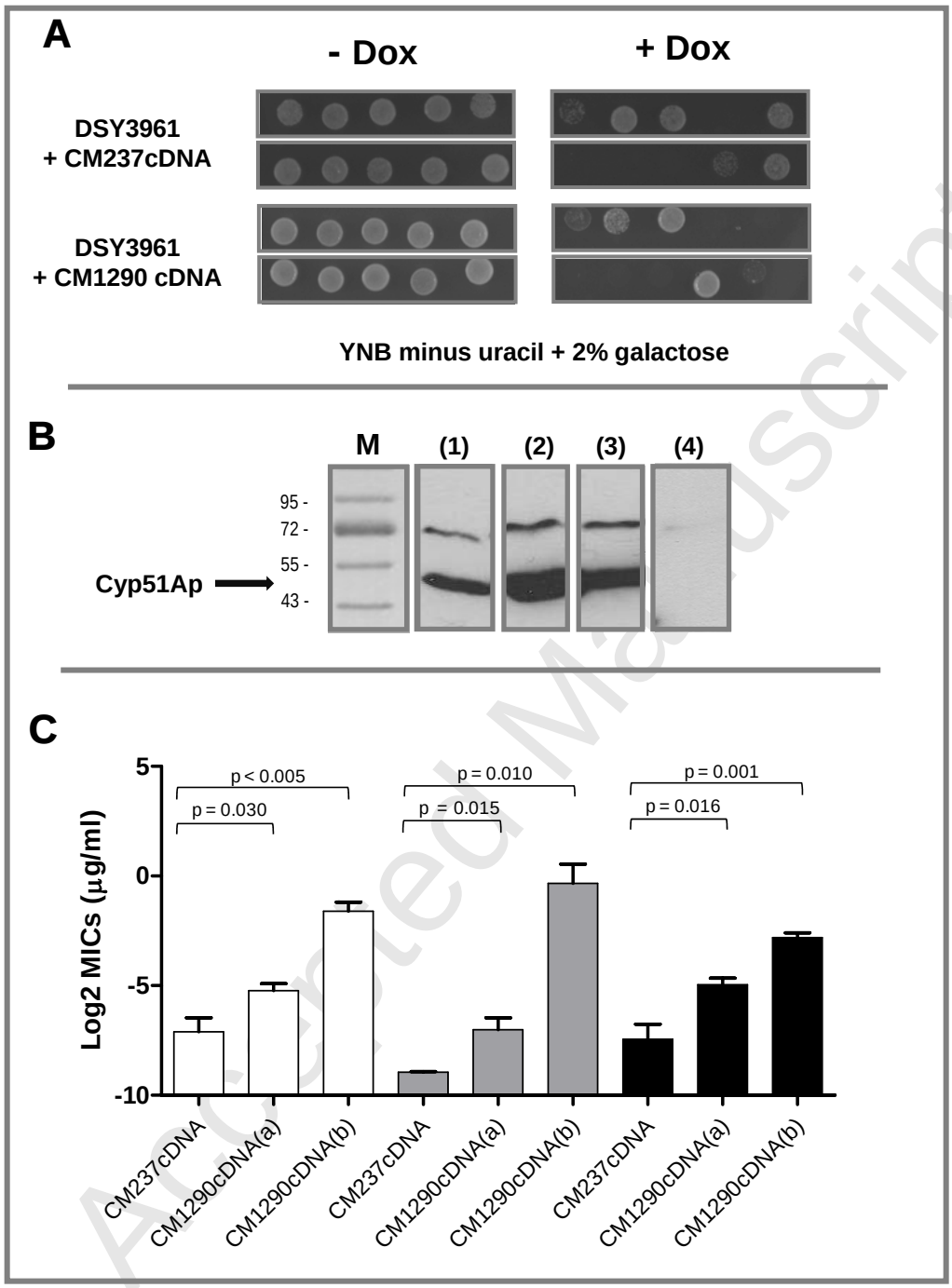

Figure 1

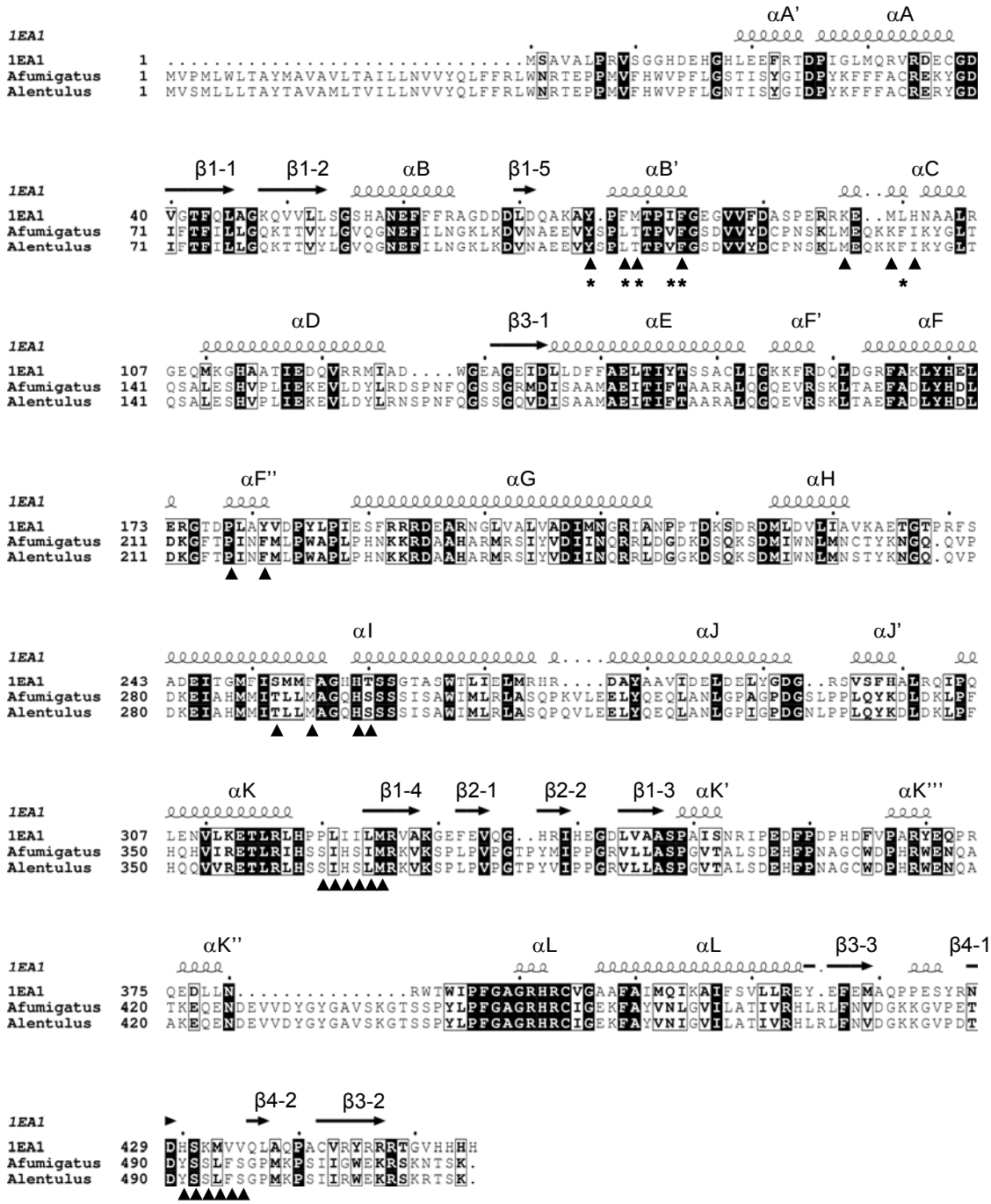
αA'
αA
1EA1
1EA1 1 ..... MSAVALPRVSGGHDEHGHLEEFRTDPIGLMQRVRDECGD
Afumigatus 1 MVPMLWLTAYMAVAVLTAILLNVVYQLFFRLWNRTEPPMVFHWVPFLGSTISYGIDPYKFFFACREKYGD
Alentulus 1 MVSMLLLTAYTAVAMLTVILLNVVYQLFFRLWNRTEPPMVFHWVPFLGNTISYGIDPYKFFFACREKYGD
β1-1
β1-2
αB
β1-5
αB'
αC
1EA1 40 VGTFQLAGKQVVLLSGSHANEFFFRAGDDDLDQAKAY.PFMTPIFGEGVVFDASPERRKE..MLHNAALR
Afumigatus 71 IFTFILLGQKTTVYLGVQGNEFILNGKLKDVNAEEVYSPLTTPVFGSDVVYDCPNSKLMEQKKFIKYGLI
Alentulus 71 IFTFILLGQKTTVYLGVQGNEFILNGKLKDVNAEEVYSPLTTPVFGSDVVYDCPNSKLMEQKKFIKYGLI
αD
β3-1
αE
αF'
αF
1EA1 107 GEQMKGHAATIEDQVRRMIAD....WGEAGEIDLLDFFAELTIYTSSACLIGKKFRDQLDGRFAKLYHEL
Afumigatus 141 QSALESHVPLIEKEVLDYLRDSPNFQGSSGRMDISAAMAEITIFTAARALQGQEVRSKLTAEFADLYHDL
Alentulus 141 QSALESHVPLIEKEVLDYLRNSPNFQGSSGQVDISAAMAEITIFTAARALQGQEVRSKLTAEFADLYHDL
αF''
αG
αH
1EA1 173 ERGTDPLAYVDPYLPIESFRRRDEARNGLVALVADIMNGRIANPPTDKSDRDMLDVLIAVKAETGTPRFS
Afumigatus 211 DKGFTPINFMLPWAPLPHNKKRDAAHARMRSIYVDIINQRRLDGDKDSQKSDMIWNLMNCTYKNGQ.QVP
Alentulus 211 DKGFTPINFMLPWAPLPHNKKRDAAHARMRSIYVDIINQRRLDGGKDSQKSDMIWNLMNSTYKNGQ.QVP
αI
αJ
αJ'
1EA1 243 ADEITGMFISMMFAGHTSSGTASWTLIELMRHR....DAYAAVIDELDELYGDG..RSVSFHALRQIPQ
Afumigatus 280 DKEIAHMMITLLMAGQHSSSSISAWIMLRLASQPKVLEELYQEQLANLGPAGPDGSLPPLQYKDLDKLPF
Alentulus 280 DKEIAHMMITLLMAGQHSSSSISAWIMLRLASQPQVLEELYQEQLANLGPIGPDGNLPPLQYKDLDKLPF
αK
β1-4
β2-1
β2-2
β1-3
αK'
αK'''
1EA1 307 LENVLKETLRLHPPLIILMRVAKGEFEVQG..HRIHEGDLVAASPAISNRIPEDFPDPHDFVPARYEQPR
Afumigatus 350 HQHVIRETLRIHSSIHSIMRKVKSPLPVPGTPYMIPPGRVLLASPGVTALSDEHFPNAGCWDPHRWENQA
Alentulus 350 HQQVVRETLRLHSSIHSLMRKVKSPLPVPGTPYVIPPGRVLLASPGVTALSDEHFPNAGCWDPHRWENQA
αK''
αL
αL
β3-3
β4-1
1EA1 375 QEDLLN.............RWTWIPFGAGRHRCVGAAFAIMQIKAIFSVLLREY.EFEMAQPPESYRN
Afumigatus 420 TKEQENDEVVDYGYGAVSKGTSSPYLPFGAGRHRCIGEKFAYVNLGVILATIVRHLRLFNVDGKKGVPET
Alentulus 420 AKEQENDEVVDYGYGAVSKGTSSPYLPFGAGRHRCIGEKFAYVNIGVILATIVRHLRLFNVDGKKGVPDT
β4-2
β3-2
1EA1 429 DHSKMVVQLAQPACVRYRRRTGVHHHH
Afumigatus 490 DYSSLFSGPMKPSIIGWEKRSKNTSK.
Alentulus 490 DYSSLFSGPMKPSIIRWEKRSKRTSK.

Figure 2.

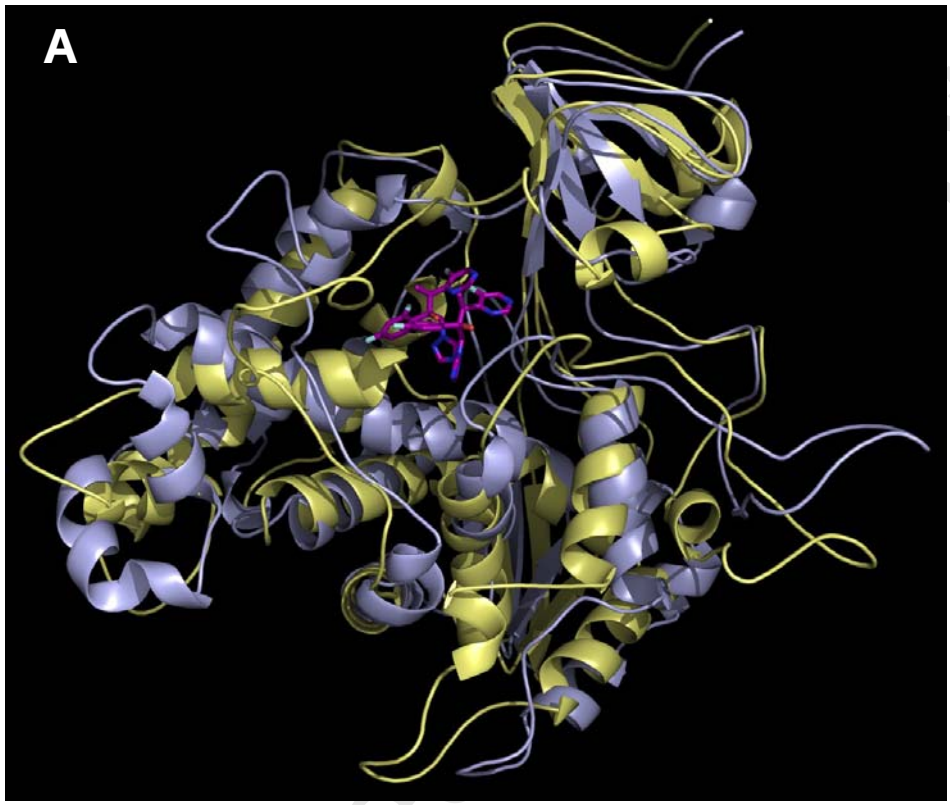

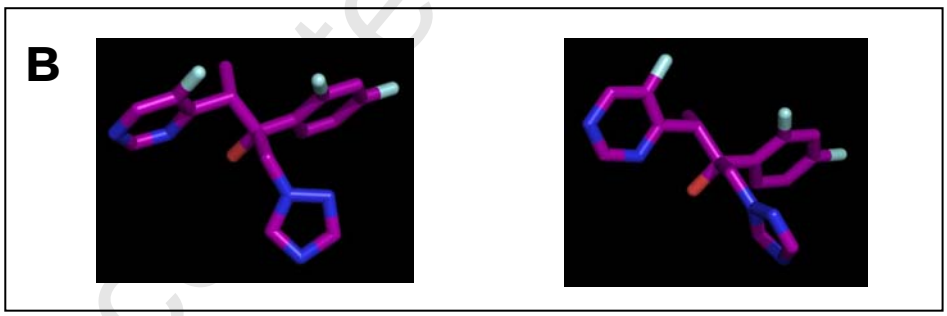

Figure 3

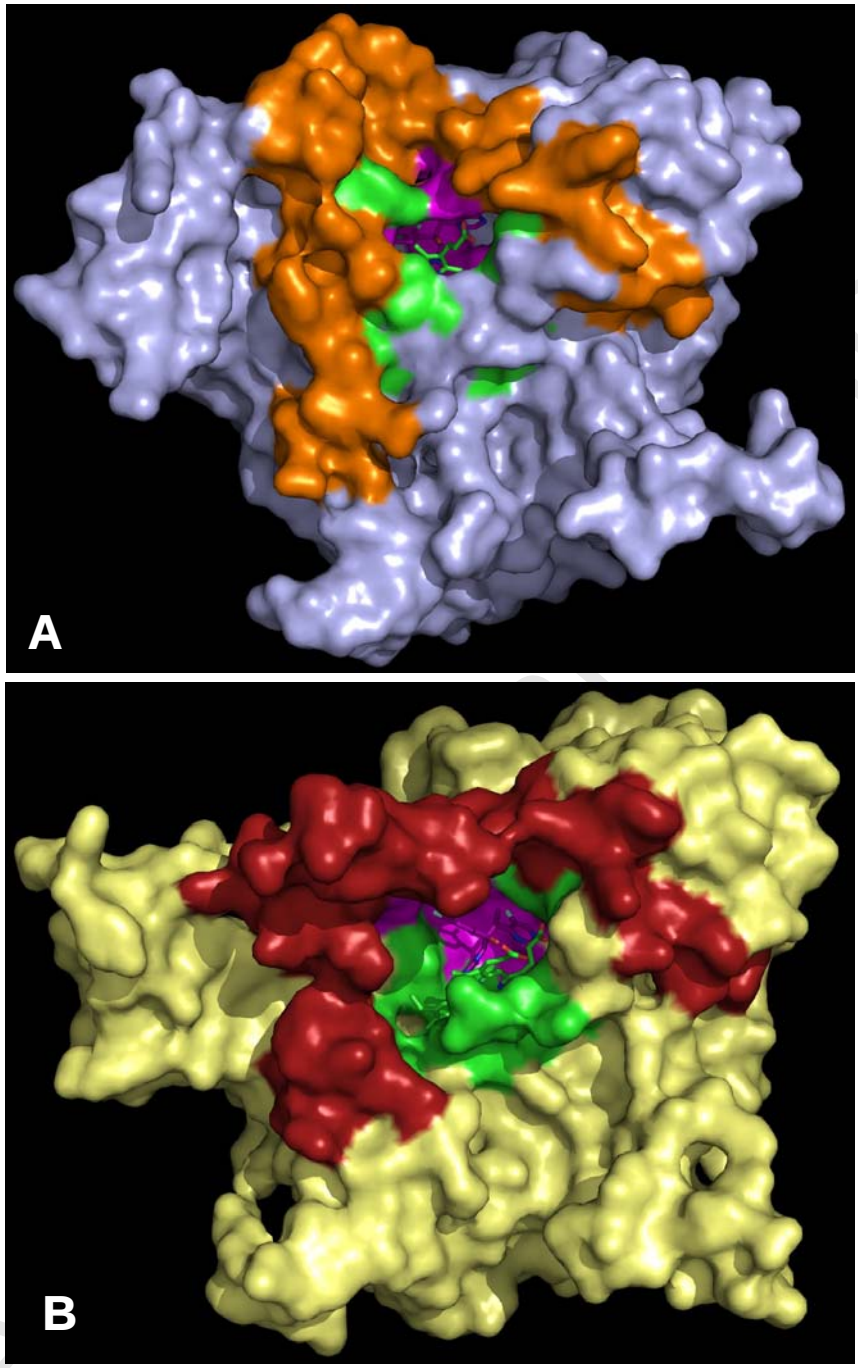

Figure 4

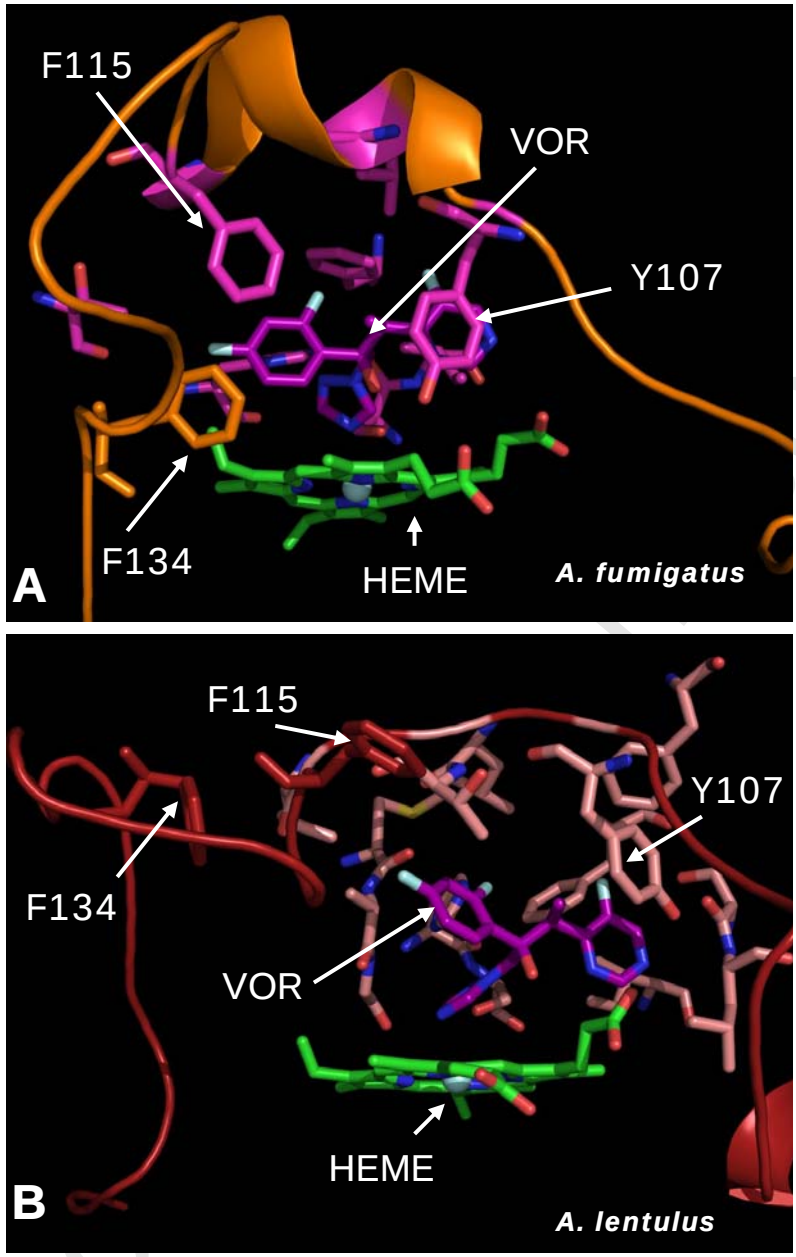
F115
VOR
Y107
F134
HEME
A
A. fumigatus
F115
Y107
F134
VOR
HEME
B
A. lentulus

Figure 5

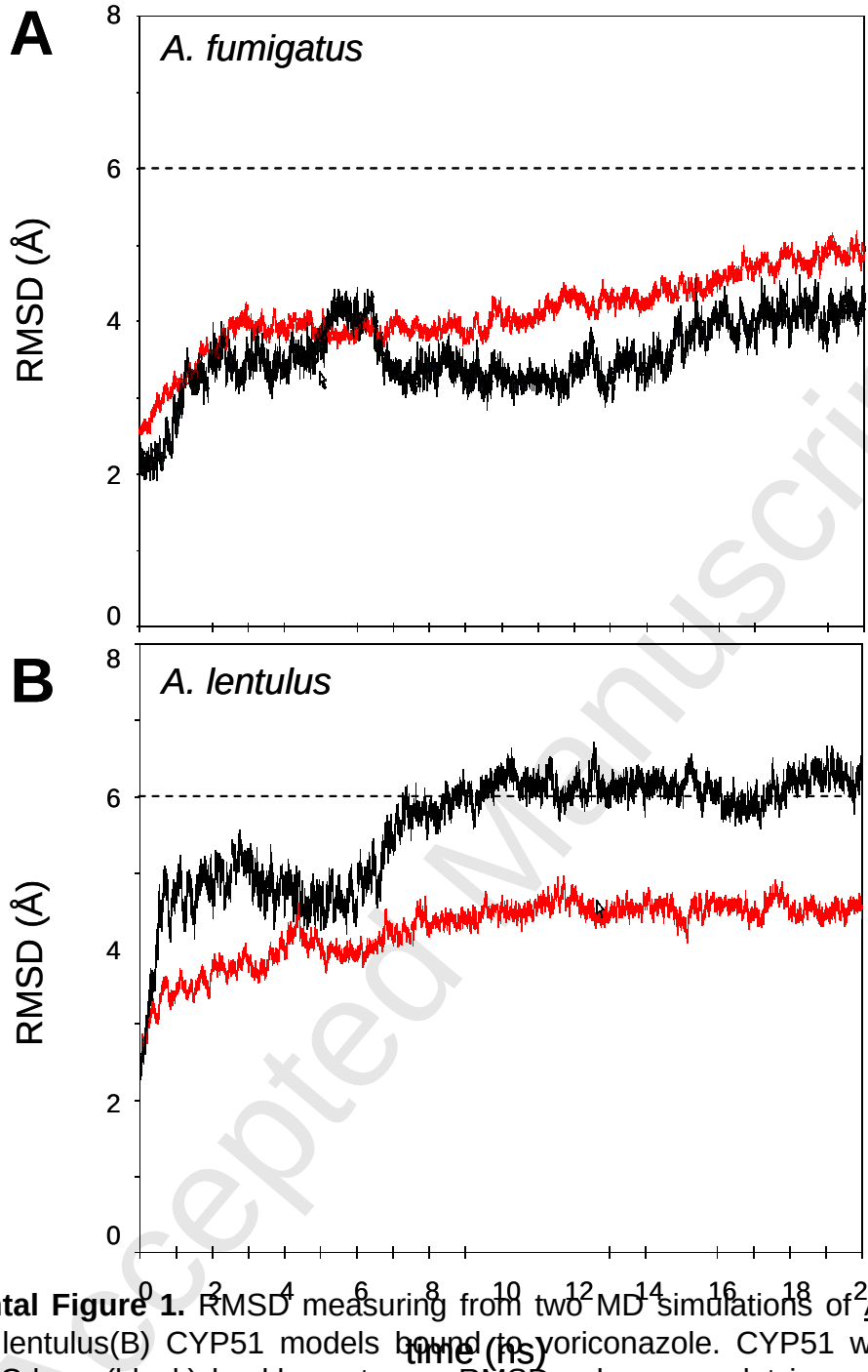

Supplemental Figure 1. RMSD measuring from two MD simulations of A. fumigatus (A) and A. lentulus(B) CYP51 models bound to voriconazole. CYP51 whole protein (red) and BC-loop (black) backbone traces RMSD values are plot in each panel. All values were calculated along a single 20 ns MD trajectory for each organism's model, taking as reference structure their respective comparative models based in CYP51 in complex with azole inhibitors from Mycobacterium tuberculosis (PDB:1EA1). In terms of RMSD, the whole backbone structure changes similarly in both models and remains stabilized during the last nanoseconds of simulation (red lines). In contrast, while the structure of the BC loop in A. fumigatus varies in a similar amount to the whole protein structure during the MD simulation (black line, upper panel), the same loop in A. lentulus (black line, lower panel) exhibits a more pronounced movement (RMSD values higher than 6 Å) that results in the differentiated open position of A. lentulus BC loop showed in figures 4 and 5.